Optica Applicata, Vol. XLIII, No. 4, 2013
DOI: 10.5277/oa130419

The effect of Drude metal shell on the dielectric rods in two-dimensional photonic crystals

ABDOLRASOUL GHARAATI*, ZAHRA ROOZITALAB

Department of Physics, Payame Noor University, Iran

*Corresponding author: agharaati@pnu.ac.ir

In this paper, we study dispersion properties in a two- dimensional metallo-dielectric nanophotonic crystal that contains dielectric rods with metallic shell in air background with two-type structures: triangular and honeycomb, based on the modified plane wave expansion method. First, the eigenvalue equations for E polarization (TM modes) and H polarization (TE modes) are derived. We draw dispersion curves and compare them with a traditional photonic crystal. Then, the effects of different thicknesses of the metallic shell are analysed on the photonic band gap. Several metals have been studied and their influence on the band gap width is investigated. Our results show that we have large photonic band gap in TM mode when we use a metallic shell on the dielectric rod compared with a traditional photonic crystal in both structures. Also, we have large photonic band gap in TE mode in the honeycomb structure. Moreover, there is very thin photonic band gap in TE mode in the triangular structure. For both structures, the band gap width will be increased by the enhancement of thickness of the metallic shell. This enhancement in TM mode is higher than TE mode. In addition, flat bands are discovered in two-dimensional metallo-dielectric photonic band structures. All of our calculations have been done by using the Drude model of metal.

Keywords: two-dimensional metallic photonic crystal, photonic band gaps, modified plane wave expansion method.

1. Introduction

Photonic crystals (PCs) are periodically structured media with different dielectric constants. PCs can be divided into one-dimensional (1D), two-dimensional (2D) and three-dimensional (3D) structures. The 2D PC is periodic along two x and y axes, and homogeneous along the z axis [1–8]. Photonic band gap (PBG) is a range of frequency in which light cannot propagate through the structure. Also, most applications of PCs are because of its PBG. Many important applications of PCs depend on the existence of a wide frequency PBG, so it is essential to find what shape can generate the largest absolute PBG in a given structure. The structure and the shape of it play very important roles in band gap width (BGW). In the last decade, scientists have investigated the PBG of 2D PCs consisting of various structures with different shapes, *e.g.*, triangular and honeycomb structures [9, 10]. They have found that these structures can

generate the largest PBG. Here we study these structures with three refractive indices: dielectric, metallic and air. Recently a great interest has been dedicated to the study of metallo-dielectric PCs (MDPCs) [11–15]. MDPCs are defined as PCs consisting of dielectric and metal elements. Compared with traditional PCs, the MDPCs have some interesting properties. There is a wide PBG between zero and the cut-off frequency in TM mode. This is explained that TM mode can couple to longitudinal oscillations of charge along the length of the rods [1]. The inclusion of metallic components can enlarge the size of the gaps and produce flat bands [1, 11, 12, 15]. Another interesting property of MDPC is the appearance of surface plasmon polaritons (SPP). If we consider a flat interface between a metal and a dielectric material, surface waves localized on the interface appear. These waves are referred to as SPP [1]. These structures are interesting for different applications such as a practical filter [1, 2, 11], polarizer [11], antenna [16] or waveguide [11, 17], in which the dimensions of metallic PCs are smaller than the minimum dimensions of a typical dielectric PC. The modelling with more than two materials in a unit cell has been reported recently [18–21]. Here, the PBG formation in 2D MDPCs with three materials is investigated. The photonic

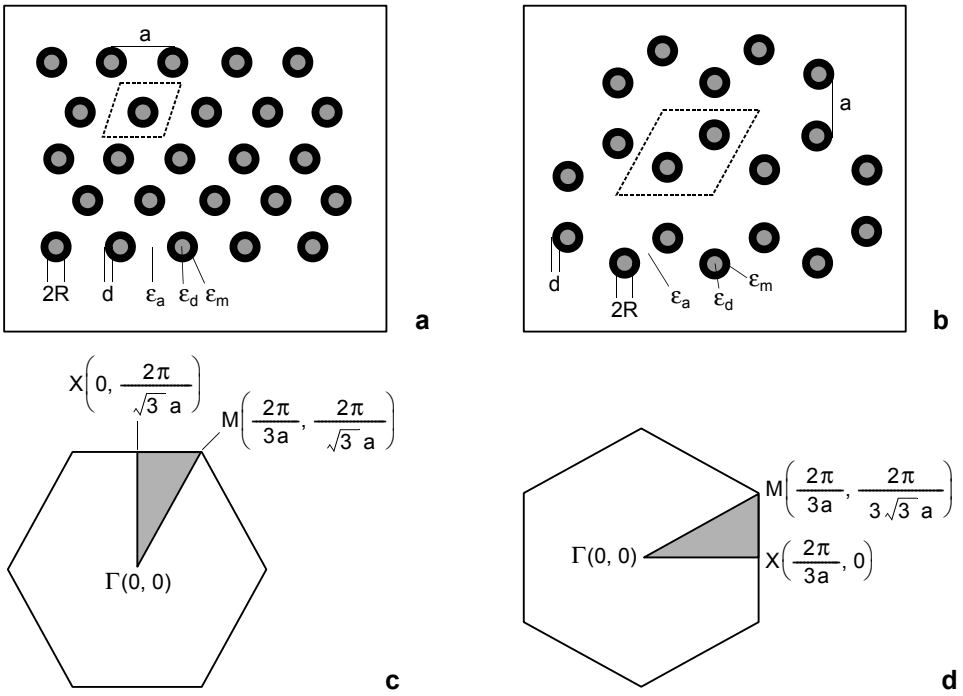

Fig. 1. Schematic structures of 2D MDPCs which contain dielectric central rods with metallic outer shell. Triangular structure (**a**), honeycomb structure (**b**), irreducible Brillouin zone of the triangular structure (**c**), and irreducible Brillouin zone of the honeycomb structure (**d**). Both structures are arranged in air background. The structure of a unit cell is indicated by a dashed line. The black, gray and white area represent metal, dielectric and air, respectively.

structure of such 2D MDPC is composed of the elements that have three indexes of refraction, *i.e.*, the background material is air with the dielectric constant ε_a and the central rods are dielectric with the dielectric constant ε_d. We assume that the third component is included as a thick cladding shell covering the central rods, this shell is metal with the dielectric constant ε_m. We calculate the photonic dispersion and analyse the effects of the metallic shell on the BGW. We have found that the existence of the metallic shell could be advantageous and cause larger PBGs.

Figure 1 shows the two types of structures, where (**a**) is a triangular structure of dielectric central rods and outer metallic shell and (**b**) is a honeycomb structure of dielectric central rods and outer metallic shell. The parameters ε_d, ε_m and ε_a are dielectric constants of the dielectric central rod, metallic shell and background, respectively. Parameters R and d are radius of central rods and thickness of the shell, respectively. The parameter a is the distance between the centres of two nearest neighbour rods. For the triangular structure, the lattice constant is equal to a, whereas for the honeycomb structure, the lattice constant is equal to $\sqrt{3}a$. The photonic band structure calculations were performed along the Γ–X–M–Γ edges of the irreducible Brillouin zone (Figs. 1**c** and 1**d**).

The rest of the paper is organized as follows. The theory which can modify plane wave expansion method (PWEM) for both modes has been presented in Section 2. Next, the dispersion curves and the influence of thickness and different metals on the PBG for two structures have been investigated in Section 3. Finally, the conclusions are given in Section 4.

2. Theoretical model

Dielectric constants of metals are frequency dependent. We have used the Drude model to describe the dielectric constant of metal as follows

$$\varepsilon_m = 1 - \frac{\omega_p^2}{\omega(\omega + i\gamma)} \tag{1}$$

where ω_p and γ are the plasma frequency and damping constant, respectively [22]. In Eq. (1), if $\omega > \omega_p$, the real part of the dielectric constant is positive and the medium is transparent. On the other hand, if $\omega < \omega_p$, the real part of the dielectric constant is negative, and the metal becomes a mirror and light cannot be transmitted. A consequence of this subject is increasing the size of the gaps and produce flat bands.

PWEM in 2D PCs is the most popular technique. In this paper, we will modify the PWEM to a standard one that is capable of analysing the 2D MDPC.

Using Maxwell's equations, we can obtain an equation in 2D PC for TM and TE modes as follows

$$\nabla \times \nabla \times E(\mathbf{r}) = \frac{\omega^2}{c^2}\varepsilon(\mathbf{r})E(\mathbf{r}) \quad \text{for TM mode} \tag{2}$$

$$\nabla \times \frac{1}{\varepsilon(\mathbf{r})} \nabla \times H(\mathbf{r}) = \frac{\omega^2}{c^2} H(\mathbf{r}) \quad \text{for TE mode} \tag{3}$$

where ω is the wave frequency, c is the speed of light in vacuum, $E(\mathbf{r})$ and $H(\mathbf{r})$ are the electric and magnetic fields, respectively, and $\varepsilon(\mathbf{r})$ is the dielectric function. The dielectric function can be expanded in the following Fourier series, TM and TE modes as:

$$\varepsilon(\mathbf{r}) = \sum_G \kappa_{\mathrm{TM}}(\mathbf{G}) \exp(i\mathbf{G} \cdot \mathbf{r}) \quad \text{for TM mode} \tag{4}$$

$$\frac{1}{\varepsilon(\mathbf{r})} = \sum_G \kappa_{\mathrm{TE}}(\mathbf{G}) \exp(i\mathbf{G} \cdot \mathbf{r}) \quad \text{for TE mode} \tag{5}$$

where $\mathbf{G}$ is the reciprocal vector; $\kappa_{\mathrm{TM}}(\mathbf{G})$ and $\kappa_{\mathrm{TE}}(\mathbf{G})$ are the Fourier coefficient of the dielectric constant for TM and TE modes. Using Bloch's theorem, $E(\mathbf{r})$ and $H(\mathbf{r})$ can be expressed as

$$E(\mathbf{r}) = \sum_G E_k(\mathbf{G}) \exp\{i(\mathbf{k} + \mathbf{G}) \cdot \mathbf{r}\} \tag{6}$$

and

$$H(\mathbf{r}) = \sum_G H_k(\mathbf{G}) \exp\{i(\mathbf{k} + \mathbf{G}) \cdot \mathbf{r}\} \tag{7}$$

where $\mathbf{k}$ is the 2D wave vector. Substituting Eqs. (6), (7) into Eqs. (2), (3), we obtain the following eigenvalue equations for the expansion coefficients

$$|\mathbf{k} + \mathbf{G}|^2 E_{z,k}(\mathbf{G}) = \frac{\omega^2}{c^2} \sum_{G'} \kappa_{\mathrm{TM}}(\mathbf{G} - \mathbf{G}') E_{z,k}(\mathbf{G}') \quad \text{for TM mode} \tag{8}$$

$$\sum_{G'} \kappa_{\mathrm{TE}}(\mathbf{G} - \mathbf{G}') |\mathbf{k} + \mathbf{G}| |\mathbf{k} + \mathbf{G}'| H_{z,k}(\mathbf{G}') = \frac{\omega^2}{c^2} H_{z,k}(\mathbf{G}) \quad \text{for TE mode} \tag{9}$$

where $E_{z,k}(\mathbf{G})$ and $H_{z,k}(\mathbf{G})$ are the Fourier coefficients of the electric and magnetic field, respectively.

First, we derive the Fourier coefficients $\kappa_{\mathrm{TM}}(\mathbf{G})$ and $\kappa_{\mathrm{TE}}(\mathbf{G})$ which we can obtain through integration over the primitive unit cell by using Eqs. (4) and (5) for TM and TE modes, respectively. In the honeycomb structure, we have two rods in one unit cell but in the triangular structure we have one rod in one unit cell, so the Fourier coefficients of the honeycomb structure should be modified. We modified them, introducing new parameters: $P(\mathbf{G}) = \cos(\mathbf{G}(a/2))$ for the honeycomb structure and $P(\mathbf{G}) = 1$ for the triangular structure. Therefore, we can obtain Fourier coefficients as follows:

$$\kappa_{\mathrm{TM}}(\mathbf{G}) = \begin{cases} (\varepsilon_m - \varepsilon_a) 2 f_{R+d} \dfrac{J_1(\mathbf{G}(R+d))}{\mathbf{G}(R+d)} P(G) + \\ \qquad + (\varepsilon_d - \varepsilon_m) 2 f_R \dfrac{J_1(\mathbf{G}R)}{\mathbf{G}R} P(G) & \text{if } \mathbf{G} \neq \mathbf{G}' \\ (\varepsilon_m - \varepsilon_a) f_{R+d} + (\varepsilon_d - \varepsilon_m) f_R + \varepsilon_a & \text{if } \mathbf{G} = \mathbf{G}' \end{cases} \tag{10}$$

$$\kappa_{\mathrm{TE}}(\mathbf{G}) = \begin{cases} \left(\dfrac{1}{\varepsilon_m} - \dfrac{1}{\varepsilon_a}\right) 2 f_{R+d} \dfrac{J_1(\mathbf{G}(R+d))}{\mathbf{G}(R+d)} P(G) + \\ \qquad + \left(\dfrac{1}{\varepsilon_d} - \dfrac{1}{\varepsilon_m}\right) 2 f_R \dfrac{J_1(\mathbf{G}R)}{\mathbf{G}R} P(G) & \text{if } \mathbf{G} \neq \mathbf{G}' \\ \left(\dfrac{1}{\varepsilon_m} - \dfrac{1}{\varepsilon_a}\right) f_{R+d} + \left(\dfrac{1}{\varepsilon_d} - \dfrac{1}{\varepsilon_m}\right) f_R + \dfrac{1}{\varepsilon_a} & \text{if } \mathbf{G} = \mathbf{G}' \end{cases} \tag{11}$$

parameters $f_{(R+d)}$ and f_R are $2\pi(R+d)^2/\sqrt{3}a^2$ and $2\pi R^2/\sqrt{3}a^2$ in the triangular structure, and $4\pi\sqrt{3}(R+d)^2/9a^2$ and $4\pi\sqrt{3}R^2/9a^2$ in the honeycomb structure, respectively.

If Equation (10) is substituted into Eq. (8) to make the transposition, the eigenvalue equation of TM mode can be obtained

$$\sum_{\mathbf{G}'} \left(-\frac{\omega^3}{c^3} - A_{\mathrm{TM}} \frac{\omega^2}{c^2} + B_{\mathrm{TM}} \frac{\omega}{c} + C_{\mathrm{TM}} \right) E_{z,k}(\mathbf{G}') = 0 \tag{12}$$

The complete solution of Eq. (12) is obtained by solving the eigenvalue equation by diagonalization of the matrix, whose eigenvalues are ω/c. For different wave vectors k, one can obtain a series of eigenfrequencies ω, which form the band structures of 2D MDPC for TM mode. This matrix is

$$\begin{bmatrix} 0 & I & 0 \\ 0 & -A_{\mathrm{TM}} & I \\ C_{\mathrm{TM}} & B_{\mathrm{TM}} & 0 \end{bmatrix} \tag{13}$$

where the elements of the matrices A_{TM}, B_{TM} and C_{TM} are given by

$$A_{\mathrm{TM}} = \frac{i\gamma}{c} I \tag{14a}$$

$$B_{\mathrm{TM}} = N^{-1}M \tag{14b}$$

$$C_{\mathrm{TM}} = N^{-1}\frac{i\gamma}{c}|k+\mathbf{G}|^2 \tag{14c}$$

$$M = \begin{cases} \dfrac{\omega_p^2}{c^2}2f_{R+d}\dfrac{J_1(|\mathbf{G}-\mathbf{G}'|(R+d))}{|\mathbf{G}-\mathbf{G}'|(R+d)}P(|\mathbf{G}-\mathbf{G}'|) + \\ \qquad -\dfrac{\omega_p^2}{c^2}2f_R\dfrac{J_1(|\mathbf{G}-\mathbf{G}'|R)}{|\mathbf{G}-\mathbf{G}'|R}P(|\mathbf{G}-\mathbf{G}'|) & \text{if } \mathbf{G}\neq\mathbf{G}' \\ |\mathbf{k}+\mathbf{G}|^2 + (f_{R+d}-f_R)\dfrac{\omega_p^2}{c^2} & \text{if } \mathbf{G}=\mathbf{G}' \end{cases} \tag{14d}$$

$$N = \begin{cases} (1-\varepsilon_a)2f_{R+d}\dfrac{J_1(|\mathbf{G}-\mathbf{G}'|(R+d))}{|\mathbf{G}-\mathbf{G}'|(R+d)}P(|\mathbf{G}-\mathbf{G}'|) + \\ \qquad +(\varepsilon_d-1)2f_R\dfrac{J_1(|\mathbf{G}-\mathbf{G}'|R)}{|\mathbf{G}-\mathbf{G}'|R}P(|\mathbf{G}-\mathbf{G}'|) & \text{if } \mathbf{G}\neq\mathbf{G}' \\ (1-\varepsilon_a)f_{R+d}+(\varepsilon_d-1)f_R+\varepsilon_a & \text{if } \mathbf{G}=\mathbf{G}' \end{cases} \tag{14e}$$

$$I = \delta_{\mathbf{G},\,\mathbf{G}'} \tag{14f}$$

Like the TM mode, we can write the eigenvalue equation of TE mode as follows,

$$\sum_{\mathbf{G}'}\left(\frac{\omega^4}{c^4}+A_{\mathrm{TE}}\frac{\omega^3}{c^3}-B_{\mathrm{TE}}\frac{\omega^2}{c^2}-C_{\mathrm{TE}}\frac{\omega}{c}+D_{\mathrm{TE}}\right)H_{z,\,k}(\mathbf{G}') = 0 \tag{15}$$

The complete solution of Eq. (15) is obtained by solving the eigenvalues of the following matrix and by the diagonalization of this matrix. The eigenvalues of this matrix are ω/c. We can obtain a series of eigenfrequencies ω for different wave vectors k, which form the band structures of 2D MDPC for TE mode. This matrix is

$$\begin{bmatrix} 0 & I & 0 & 0 \\ 0 & 0 & I & 0 \\ 0 & B_{\mathrm{TE}} & -A_{\mathrm{TE}} & I \\ -D_{\mathrm{TE}} & C_{\mathrm{TE}} & 0 & 0 \end{bmatrix} \tag{16}$$

where the elements of the matrices A_{TE}, B_{TE}, C_{TE} and D_{TE} are:

$$A_{\mathrm{TE}} = \frac{i\gamma}{c}I \tag{17a}$$

$$B_{\mathrm{TE}} = \begin{cases} \left[\left(1-\frac{1}{\varepsilon_a}\right)2f_{R+d}\frac{J_1(|\mathbf{G}-\mathbf{G}'|(R+d))}{|\mathbf{G}-\mathbf{G}'|(R+d)}P(|\mathbf{G}-\mathbf{G}'|) + \right. & \\ \left. +\left(\frac{1}{\varepsilon_d}-1\right)2f_R\frac{J_1(|\mathbf{G}-\mathbf{G}'|R)}{|\mathbf{G}-\mathbf{G}'|R}P(|\mathbf{G}-\mathbf{G}'|)\right]|\mathbf{k}+\mathbf{G}||\mathbf{k}+\mathbf{G}'| & \text{if } \mathbf{G}\neq\mathbf{G}' \\ \left[\frac{1}{\varepsilon_a}+\left(1-\frac{1}{\varepsilon_a}\right)f_{R+d}+\left(\frac{1}{\varepsilon_d}-1\right)f_R\right]|\mathbf{k}+\mathbf{G}||\mathbf{k}+\mathbf{G}'|+\frac{\omega_p^2}{c^2} & \text{if } \mathbf{G}=\mathbf{G}' \end{cases} \tag{17b}$$

$$C_{\mathrm{TE}} = \begin{cases} \frac{i\gamma}{c}\left[\left(1-\frac{1}{\varepsilon_a}\right)2f_{R+d}\frac{J_1(|\mathbf{G}-\mathbf{G}'|(R+d))}{|\mathbf{G}-\mathbf{G}'|(R+d)}P(|\mathbf{G}-\mathbf{G}'|) + \right. & \\ \left. +\left(\frac{1}{\varepsilon_d}-1\right)2f_R\frac{J_1(|\mathbf{G}-\mathbf{G}'|R)}{|\mathbf{G}-\mathbf{G}'|R}P(|\mathbf{G}-\mathbf{G}'|)\right] & \text{if } \mathbf{G}\neq\mathbf{G}' \\ \frac{i\gamma}{c}\left[\frac{1}{\varepsilon_a}+\left(1-\frac{1}{\varepsilon_a}\right)f_{R+d}+\left(\frac{1}{\varepsilon_d}-1\right)f_R\right] & \text{if } \mathbf{G}=\mathbf{G}' \end{cases} \tag{17c}$$

$$D_{\mathrm{TE}} = \begin{cases} \frac{\omega_p^2}{c^2}\left[-\frac{1}{\varepsilon_a}2f_{R+d}\frac{J_1(|\mathbf{G}-\mathbf{G}'|(R+d))}{|\mathbf{G}-\mathbf{G}'|(R+d)}P(|\mathbf{G}-\mathbf{G}'|) + \right. & \\ \left. +\frac{1}{\varepsilon_d}2f_R\frac{J_1(|\mathbf{G}-\mathbf{G}'|R)}{|\mathbf{G}-\mathbf{G}'|R}P(|\mathbf{G}-\mathbf{G}'|)\right]|\mathbf{k}+\mathbf{G}||\mathbf{k}+\mathbf{G}'| & \text{if } \mathbf{G}\neq\mathbf{G}' \\ \frac{\omega_p^2}{c^2}\left[\frac{1}{\varepsilon_a}+\left(-\frac{1}{\varepsilon_a}\right)f_{R+d}+\frac{1}{\varepsilon_d}f_R\right]|\mathbf{k}+\mathbf{G}||\mathbf{k}+\mathbf{G}'| & \text{if } \mathbf{G}=\mathbf{G}' \end{cases} \tag{17d}$$

3. Results and discussion

In this section, in order to compare our results with traditional PCs for both structures, we calculate the dispersion curves for two thicknesses, with and without a shell, *i.e.*, $d = 0.2a$, and $d = 0$. Traditional PCs have been studied theoretically for both structures as in Ref. [3, 10, 23].

In this paper, the dielectric rod is taken to be alumina in which the dielectric constant is $\varepsilon_d = 8.9$ [2] and metallic shell is silver (Ag) with the plasma frequency and

T a b l e 1. The BGR in TM and TE modes for the triangular structure in a unit of $\omega a/2\pi c$.

BGR	$TM_{0\text{-}1}$	$TM_{1\text{-}2}$	$TM_{2\text{-}3}$	$TM_{3\text{-}4}$	$TE_{13\text{-}14}$
Triangular structure	0–0.53	0.53–0.85	0.85–1.16	1.16–1.25	0.72–0.75

T a b l e 2. The BGR in TM and TE modes for the honeycomb structure in a unit of $\omega a/2\pi c$.

BGR	$TM_{0\text{-}1}$	$TM_{2\text{-}3}$	$TM_{4\text{-}5}$	$TM_{11\text{-}12}$	$TE_{3\text{-}4}$
Honeycomb structure	0–0.53	0.55–0.87	0.868–1.14	1.33–1.48	0.22–0.335

damping constant, $\omega_p = 2\pi\times2.175\times10^{15}$ rad/s and $\gamma = 2\pi\times4.35\times10^{12}$ rad/s, respectively [24]. For both structures, the background is air with the dielectric constant $\varepsilon_a = 1$ and $a = 500$ nm. The situation for TM mode was different from TE mode. A finite cut-off frequency was observed for TM mode. These cut-off frequencies for both structures are $0.53(\omega a/2\pi c)$ that is equivalent to 3.18×10^{14} Hz. However, for the case of both modes, when the thickness of metal coating is thick, the convergence of calculation is slow with an increasing number of plane waves because of the existence of surface plasmon modes. In this paper, a total of 441 plane waves are used to obtain the results for TM and TE modes [25, 26]. For these modes, we should note that there exist several flat bands in the band structure of 2D MDPCs.The spectral region of flat bands for triangular and honeycomb lattices in both modes can be observed in Figs. 2**a**, 3**a**, 4**a** and 5**a**, respectively (red color). Those bands with extremely flat dispersion that originates from the two SPPs are located in this frequency range. We give the ranges of PBGs for TM and TE modes in tringular and honeycomb structures, in Tabs. 1 and 2, respectively.

3.1. Dispersion curves

We draw dispersion curves of TM and TE modes by calculating photonic bands by solving Eqs. (12) and (15). As the solution of Eqs. (12) and (15) is very difficult, the Matlab program cannot solve it. We guess the matrices (13) and (16) as their eigenvalues are the answers to Eqs. (12) and (15), respectively, [12, 27]. Now, by using the Matlab program, we obtain the eigenvalues of matrices (13) and (16) which are ω/c. We can obtain a series of eigenfrequencies ω for different wave vectors k, which form the band structures.

Figure 2 has shown dispersion curves with different thicknesses of the metallic shell for TM mode in the triangular structure. The thickness of the metallic shell and the radius of the central rod in Figs. 2**a** and 2**b** are $d = 0.2a$, $R = 0.2a$ and $d = 0$, $R = 0.4a$, respectively. The structure in Fig. 2**a** leads to five flat bands and four large PBGs; $TM_{0\text{-}1}$ (the gap between the zero frequency and the cut-off frequency), $TM_{1\text{-}2}$, $TM_{2\text{-}3}$ and $TM_{3\text{-}4}$. In Figure 2**b**, when in Eq. (10) we substitute $d = 0$, the structure

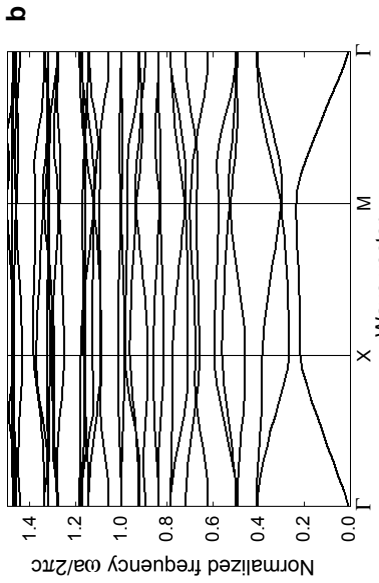

Fig. 2. Comparing dispersion curves for TM mode in the triangular structure with the thickness of the metallic shell and the radius of an alumina rod: $d = 0.2a$, $R = 0.2a$ (**a**) and $d = 0$, $R = 0.4a$ (**b**).

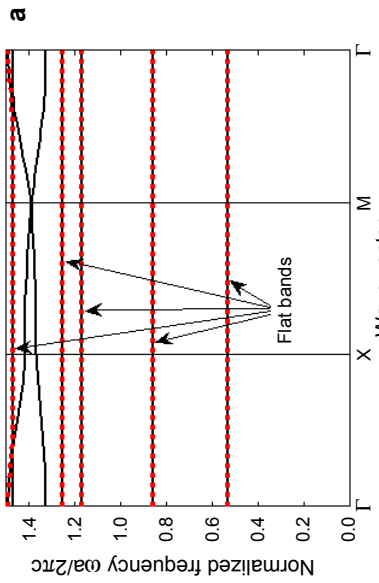

Fig. 3. Comparing dispersion curves in TM mode in the honeycomb structure with the thickness of the metallic shell and the radius of an alumina rod: $d = 0.2a$, $R = 0.2a$ (**a**) and $d = 0$, $R = 0.4a$ (**b**).

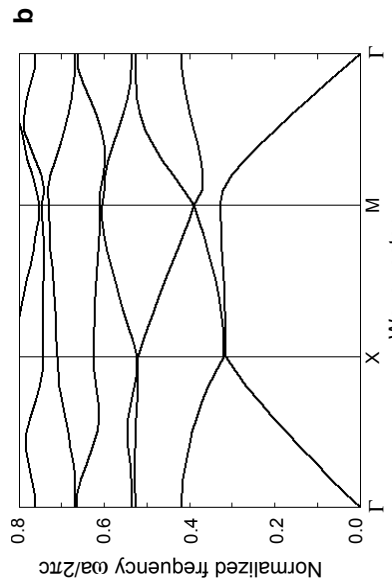

Fig. 4. Comparing dispersion curves in TE mode in the triangular structure with the thickness of the metallic shell and the radius of an alumina rod: $d = 0.2a$, $R = 0.2a$ (**a**) and $d = 0$, $R = 0.4a$ (**b**).

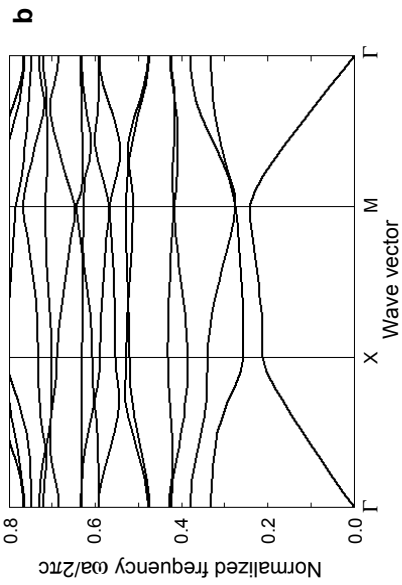

Fig. 5. Comparing dispersion curves in TE mode in the honeycomb structure with the thickness of the metallic shell and the radius of an alumina rod: $d = 0.2a$, $R = 0.2a$ (**a**) and $d = 0$, $R = 0.4a$ (**b**).

becomes PC containing an alumina rod with the radius $R = 0.4a$ that arranges in air with the triangular structure.

Figure 3 is the same as Fig. 2 but in the honeycomb structure. In Figure 3**a**, the structure leads to seven flat bands and four large PBGs; $TM_{0\text{-}1}$, $TM_{2\text{-}3}$, $TM_{4\text{-}5}$ and $TM_{11\text{-}12}$. In Figure 3**b**, when in Eq. (10) we substitute $d = 0$, the structure becomes PCs containing an alumina rod with the radius $R = 0.4a$ that arranges in air with the honeycomb structure.

Figures 4 and 5 have shown dispersion curves with different thicknesses of the metallic shell for TE mode in the triangular and honeycomb structures, respectively. The thickness of the metallic shell and the radius of an alumina rod are: $d = 0.2a$, $R = 0.2a$ (Figs. 4**a** and 5**a**) and $d = 0$, $R = 0.4a$ (Figs. 4**b** and 5**b**).

In Figures 4**b** and 5**b**, when in Eq. (11) we substitute $d = 0$, the structure becomes an alumina rod with the radius $R = 0.4a$ that arranges in air background with the triangular and honeycomb structures, respectively. When this alumina rod with the radius $R = 0.2a$ in the triangular structure has been cladded by silver with $d = 0.2a$, the structure has very thin PBG ($TE_{13\text{-}14}$) and one flat band in TE mode (Fig. 4**a**). But, the silver shell leads to one large PBG ($TE_{3\text{-}4}$) and two flat bands in the honeycomb structure (Fig. 5**a**). The range of $TE_{3\text{-}4}$ is $(0.22–0.335(\omega a/2\pi c))$.

We give the ranges of BGs (BGR) in TM and TE modes in the tringular and honeycomb structures, in Tables 1 and 2, respectively.

3.2. The effect of the thickness of the metallic shell on BGW

The gap maps in Figs. 6**a** and 6**b** have shown the effect of different thicknesses of the metallic shell on the PBG for both modes in the triangular and honeycomb structures, respectively. As the thickness of the metallic shell increases, the BGW becomes larger, for both modes and in both structures.This increasing in TM mode is

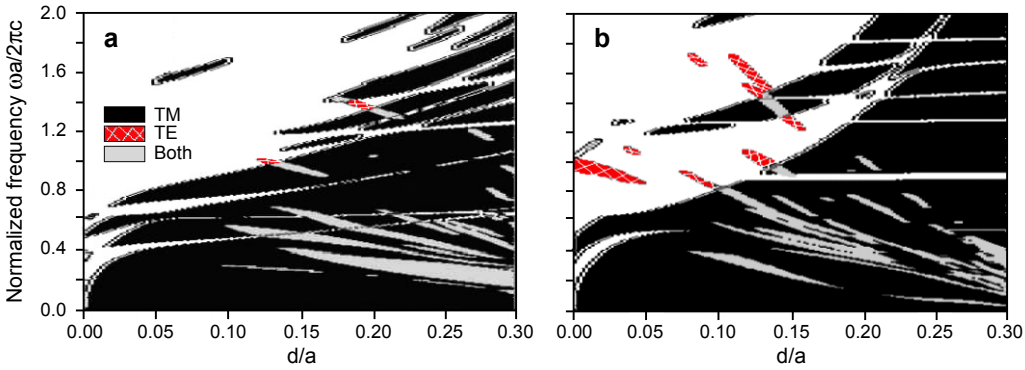

Fig. 6. Gap maps for 2D MDPCs in triangular (**a**) and honeycomb (**b**) structure. Radius of an alumina rod is $R = 0.2a$, where a is 500 nm, dielectric constant of an alumina rod and air background are $\varepsilon_d = 8.9$ and $\varepsilon_a = 1$, respectively.

T a b l e 3. The BGW for different metallic shells in the triangular structure in a unit of $\omega a/2\pi c$.

Metallic shell	TM_{0-1}	TM_{1-2}	TM_{2-3}	TM_{3-4}	TE_{13-14}
Copper	0.52	0.32	0.30	0.08	0.032
Gold	0.53	0.3264	0.31	0.082	0.032
Aluminium	0.568	0.3414	0.3156	0.092	0.0324

T a b l e 4. The BGW for different metallic shells in the honeycomb structure in a unit of $\omega a/2\pi c$.

Metallic shell	TM_{0-1}	TM_{2-3}	TM_{4-5}	TM_{11-12}	TE_{3-4}
Copper	0.52	0.3162	0.263	0.117	0.11
Gold	0.532	0.3205	0.26	0.146	0.145
Aluminium	0.5649	0.3224	0.2657	0.154	0.16

higher than in TE mode. The PBGs in TM mode shift towards higher frequency but in TE mode they shift towards lower frequency. In Figure 6 the black, cross sign (red color) and grey areas represent the PBG for TM, TE and both modes, respectively.

3.3. The effect of different metals on BGW

In this work, we use silver as a metal for the shell. Now, copper, gold and aluminium with the plasma frequency $\omega_p = 2\pi\times1.914\times10^{15}$, $2\pi\times2.18\times10^{15}$, $2\pi\times3.57\times10^{15}$ rad/s and the damping constant $\gamma = 2\pi\times8.34\times10^{12}$, $2\pi\times6.5\times10^{12}$, $2\pi\times19.4\times10^{12}$ rad/s, respectively [24], have been used in both structures.

We give the BGWs for both modes in the tringular and honeycomb structures with different metallic shells in Tabs. 3 and 4, respectively. In all cases, the radius of an alumina rod is $R = 0.2a$, where a is 500 nm, the dielectric constant of an alumina rod and air background are $\varepsilon_d = 8.9$ and $\varepsilon_a = 1$, respectively. Large PBGs would be obtained for aluminium because the plasma frequency of aluminium is higher than in other metals. This can be explained by considering the skin depth in plasma. The skin depth for static modes in plasma is given by $\delta = c/\omega_p$ [22], where c is the speed of light in vacuum. As ω_p becomes larger, the skin depth becomes smaller and the coupling between dielectrics becomes weaker, so large PBG appears. But aluminium has a big loss and is not recommended for photonic crystals [24]; silver and gold are acceptable among the above mentioned metals because they have large PBG and a small loss.

4. Conclusions

In this paper, different dispersion properties of 2D MDPC in two structures, triangular and honeycomb, are studied with the use modified PWEM. Results have shown that when we use a metallic shell on the dielectric rod instead of any other shells, PBGs in the triangular structure become larger in TM mode and there is a very thin PBG in TE mode, and PBGs in the honeycomb structure become larger in TM and TE modes.

It is worth noting that larger gaps for TM mode will appear for both structures while larger gaps for TE mode will appear for the honeycomb structure than in the triangular structure, when other parameters are the same. In addition, the flat bands are discovered in 2D MD photonic band structures. For both modes, bands in the honeycomb lattice are more flat than the triangular lattice. By comparing our results with other [3, 10, 23, 26], we can discover that when we consider a thick metallic shell, damping constant and honeycomb lattices, then the flat bands and PBG are much better than in previous publications.

For both structures, the BGW will be increased by the enhancement of the thickness of a metallic shell, but this enhancement in TM mode is higher than in TE mode. Also, it has been observed that the PBGs in the TM mode shift towards higher frequencies and for TE mode shift towards lower frequencies when the thickness of a metallic shell in both structures increases. Comparing the results for different metals, we have found that silver and gold are acceptable in all cases for PCs. Therefore, by carefully selecting the thickness and kind of metallic shells for the two structures of 2D MDPC, moderate PBG structures can be obtained. These results may provide theoretical instructions for designing new PC devices using metallic-dielectric structures.

Acknowledgments – This work has been financially supported by the Payame Noor University (PNU).

References

[1] Sakoda K., *Optical Properties of Photonic Crystals*, 2nd Edition, Springer-Verlag, Berlin, 2001.
[2] Joannopoulos J.D., Meade R.D.,Winn J.N., *Photonic Crystals: Molding the Flow of Light*, 2nd Edition, Princeton University Press, Princeton, 1995.
[3] Johnson S.G., Joannopoulos J.D., *Introduction to photonic crystals: Bloch's theorem, band diagrams and gaps (but no defects)*, 2003; http://ab-initio.mit.edu/photons/tutorial/
[4] Sukhoivanov A., Guryev V., *Photonic Crystals*, Springer-Verlag, Berlin, 2009.
[5] Shampert J.D., *Modeling of Periodic Dielectric Structures*, University of Michigan, 2001.
[6] Ozbay E., Bulu I., Aydin K., Caglayan H., Guven K., *Physics and applications of photonic crystals*, Photonics and Nanostructures – Fundamentals and Applications **2**(2), 2004, pp. 87–95.
[7] Skorobogatiy M., Yang J., *Fundamentals of Photonic Crystal Guiding*, Cambridge University Press, 2009.
[8] Yasumoto K., *Electromagnetic Theory and Application for Photonic Crystals*, Kyushu University, 2006.
[9] Weimin Kuang, Zhilin Hou, Youyan Liu, Hai Li, *The bandgap of a photonic crystal with triangular dielectric rods in a honeycomb lattice*, Journal of Optics A: Pure and Applied Optics **7**(10), 2005, pp. 525–528.
[10] Kalra Y., Sinha R.K., *Modelling and design of complete photonic band gaps in two-dimensional photonic crystals*, Pramana – Journal of Physics **70**(1), 2008, pp. 153–161.
[11] Ustyantsev M.A., *Analysis and Design of Metallo-dielectric PCs*, University Rovira i Virgili, 2007.
[12] Qi L.-M., Yang Z., *Modified plane wave method analysis of dielectric plasma photonic crystal*, Progress in Electromagnetics Research **91**, 2009, pp. 319–332.
[13] Manzanares-Martinez J., *Analytic expression for the effective plasma frequency in one-dimensional metallic-dielectric photonic crystal*, Progress in Electromagnetics Research M **13**, 2010, pp. 189–202.

[14] KUMAR V., SINGH K.S., OJHA S.P., *Band structure, reflection properties and abnormal behaviour of one-dimensional plasma photonic crystals*, Progress in Electromagnetics Research M **9**, 2009, pp. 227–241.
[15] AASWATH RAMAN, SHANHUI FAN, *Photonic band structure of dispersive metamaterials formulated as a Hermitian eigenvalue problem*, Physical Review Letters **104**, 2010, article 087401.
[16] ENGHETA N., ZIOLKOWSKI R.W., *Metamaterials: Physics and Engineering Explorations*, John Wiley and Sons, 2006.
[17] KANGLIN WANG, MITTLEMAN D.M., *Guided propagation of terahertz pulses on metal wires*, Journal of the Optical Society of America B **22**(9), 2005, pp. 2001–2008.
[18] GHARAATI A., SERAJFARD A., *Analytical calculation of band gap of a 1D planar ternary photonic crystal by simulating with a symmetric lossless transmission line*, Progress in Electromagnetics Research Letters **28**, 2012, pp. 101–109.
[19] GHARAATI A., AZARSHAB H., *Characterization of defect modes in one dimensional ternary metallo-dielectric nanolayered photonic crystal*, Progress in Electromagnetics Research **37**, 2012, pp. 125–141.
[20] GHARAATI A., ZARE Z., *Photonic band structures and enhancement of omnidirectional reflection bands by using a ternary 1D photonic crystal including left-handed materials*, Progress in Electromagnetics Research M **20**, 2011, pp. 81–94.
[21] MANZANARES-MARTINEZ J., CASTRO-GARAY P., MOCTEZUMA-ENRIQUEZ D., ARCHULETA-GARCIA R., VELARDE-CHONG M.A., *Complex band structure in one-dimensional photonic heterostructures*, Advanced Studies in Theoretical Physics **4**(13–16), 2010, pp. 759–772.
[22] JACKSON J.D., *Classical Electrodynamics*, 3rd Edition, California University, 1999.
[23] TRIFONOV T., *Photonic Band Gap Analysis and Fabrication of Macroporous Silicon by Electrochemical Etching*, University Rovira i Virgili,, 2004.
[24] EL-KADY I., SIGALAS M.M., BISWAS R., HO K.M., SOUKOULIS C.M., *Metallic photonic crystals at optical wavelengths*, Physical Review B **62**, 2000, pp. 15299–15302.
[25] SHAINLINE J.M., XU J., *Slow light and band gap in metallodielectric cylinder arrays*, Optics Express **17**(11), 2009, pp. 8879–8891.
[26] CHUAN CHENG, CAN XU, *Photonic band in two-dimensional metallodielectric photonic crystals composed of metal coated cylinders*, Journal of Applied Physics **106**(3), 2009, article 033101.
[27] LOW K.L., MAT JAFRI M.Z., KHAN S.A., *Effective plasma frequency for two-dimensional metallic photonic crystals*, Progress in Electromagnetics Research M **12**, 2010, pp. 67–79.

Received January 31, 2013
in revised form May 31, 2013